Chemical Engineering Journal 238 (2014) 17–26

Contents lists available at ScienceDirect

Chemical Engineering Journal

journal homepage: www.elsevier.com/locate/cej

A new method for studying activity and reaction kinetics of photocatalytic water oxidation systems using a bubbling reactor

Simelys Hernández [a,*], Samir Bensaid [b], Marco Armandi [a], Adriano Sacco [a], Angelica Chiodoni [a], Barbara Bonelli [b], Edoardo Garrone [b], C. Fabrizio Pirri [a,b], Guido Saracco [b]

[a] Center for Space Human Robotics @POLITO, Istituto Italiano di Tecnologia, C.so Trento 21, 10129 Turin, Italy
[b] Applied Science and Technology Department, Politecnico di Torino, C.so Duca degli Abruzzi 24, 10129 Turin, Italy

HIGHLIGHTS

- A new method is proposed for studying overall activity of water oxidation catalysts.
- Mass transfer phenomena in the bubbling reactor have been mathematically modelled.
- The actual rate of oxygen formation (R_{O_2}) as a function of time is calculated.
- Increase of sweeping gas flow enhances R_{O_2} by decreasing diffusional limitations.
- The method can be also applied for testing semiconductor photocatalysts.

GRAPHICAL ABSTRACT

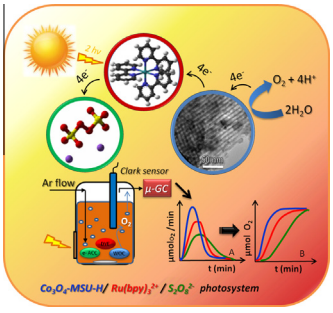

ARTICLE INFO

Article history:
Available online 5 September 2013

Keywords:
Artificial photosynthesis
Water oxidation
Bubbling reactor
Photocatalysis
Kinetic study

ABSTRACT

A novel method is proposed for studying kinetics and overall activity of water oxidation (WO) catalysts using a bubbling reactor, where oxygen concentration is measured simultaneously in the liquid and in the gaseous phase. Total oxygen evolution is obtained from direct integration. The actual rate of oxygen formation as a function of time, $R_{O_2}(t)$ not accessible to direct measurement with batch reactors, is calculated from raw data through a simple but comprehensive mathematical model, taking into account mass transfer phenomena occurring in the system. Data concerning the activity of a nanostructured Co_3O_4 catalyst dispersed on a mesoporous silica (MSU-H), in the presence of tris(2,2′-bipyridyl)Ruthenium $[Ru(bpy)_3]^{2+}$ as sensitizer and $Na_2S_2O_8$ as sacrificial reactant, are used to illustrate data processing. Behaviour of the system is complicated by the occurrence, besides WO reaction, of the degradation of the sensitizer. Increase of sweeping gas flow increases $R_{O_2}(t)$, by decreasing diffusional limitations to the reactions in the system: conditions for minimizing those were established. Data reported show that the assumption generally made of equilibrium between gaseous and liquid phase through Henry's law is incorrect, the more so the smaller the apparent mass transfer coefficient, k_La. An additional reason for removing oxygen from the liquid phase through bubbling is the occurrence of a parasitic reaction of molecular oxygen with the sensitizer. The method seems to yield reliable values of both k_La and the set of $R_{O_2}(t)$ values: the former scales with the flow of sweeping gas, as expected; $R_{O_2}(t)$ curves are in qualitative agreement with accepted reaction mechanisms. Results concerning $R_{O_2}(t)$ lend support to our previous kinetic studies (M. Armandi et al., ACS Catal, 2013, 3, 1272) where the reaction rate was assumed as constant for the first ~15 min. Availability of $R_{O_2}(t)$ data not too biased by diffusional limitations opens the way to realistic studies of the kinetic features of WO heterogeneous reactions, in the present case as well as in many others.

* Corresponding author. Tel.: +39 011 0903418.
E-mail address: simelys.hernandez@iit.it (S. Hernández).

1385-8947/$ - see front matter © 2013 Elsevier B.V. All rights reserved.
http://dx.doi.org/10.1016/j.cej.2013.08.094

Nomenclature

Symbols

b_i	GC analyzer's sampling time (s)
C_{O_2}	oxygen concentration in the liquid (mol/m^3)
$C^*_{O_2}$	oxygen concentration in equilibrium with $p_{O_2,analyzer}$ calculated by Henry's law
$CumO_2$	cumulative oxygen in all the environments of the reactor (mol)
H	O_2 Henry's law constant (m^3 Pa mol^{-1})
k_La	gas–liquid mass transfer coefficient of the oxygen (s^{-1})
P	absolute pressure in the headspace of the reactor (Pa)
$p_{O_2,b}$	oxygen partial pressure in the gaseous bubbles (Pa)
p_{O_2}	oxygen partial pressure in the gas phase above the liquid (Pa)
$p_{O_2,analyzer}$	oxygen partial pressure in the GC analyzer (Pa)
Q	Argon sweeping gas flow rate ≈ gaseous bubble flow rate (m^3 s^{-1})
R	gas perfect constant (J mol^{-1} K^{-1})
R_{O_2}	reaction rate of O_2 generation (mol m^{-3} s^{-1})
R'_{O_2}	reaction rate of O_2 generation referred to V_R (mol s^{-1})
r_{is}	reaction rate of oxygen generation in the liquid phase, in the Laplace domain (mol m^{-3} s^{-1})
t	time (s)
T	absolute temperature (K)
V_l	liquid phase volume (m^3)
V_b	gaseous bubble phase volume (m^3)
V_R	reactor volume ($V_l + V_g$) (m^3)
V_g	gas phase in the headspace above the liquid (m^3)
X	oxygen concentration in the liquid, in the Laplace domain (mol/m^3)
Y	oxygen partial pressure in the gaseous bubbles, in the Laplace domain (Pa)
Z	oxygen partial pressure in the gas phase above the liquid, in the Laplace domain (Pa)

Greek characters

ε	gaseous bubbles hold up (−)
Δt	GC measurement delay (s)
Φ_{O2}	O_2 flow rate in the gas phase (m^3 s^{-1})

Subscripts and suffixes

exp	experimental value
sim	simulated value
_L	in the liquid phase
_out	flowed out to the GC analyzer
_gen	generated
_G	in the headspace above the liquid

Units are expressed as used in the equations; units in the figures are coherent with the captions.

1. Introduction

Researchers all over the world are investigating photochemical water splitting (WS) to H_2 and O_2, as a promising way to store solar energy [1], a challenging reaction thermodynamically uphill [2]. Hydrogen can then be used directly in combustion engines or fuel cells, or combined catalytically with CO_2 to make carbon containing fuels [2,3].

WS on semiconductors has been much studied since the pioneering work by Honda and Fujishima [4] with a TiO_2 photoelectrode under UV illumination. The wide band gap, however, of common semiconductors hampers their efficiency, since the absorption of the solar energy is limited to a tiny fraction of the total [5], basically in the UV. Thus, many new semiconductors are being studied [6].

A common approach consists in separating the functions of light harvesting from water oxidation (WO) and hydrogen formation [7]. As it concerns WO, different metal oxides (containing Ir, Co, Ru, Ni, Rh and Mn) and transition metal complexes (basically Co- and Ru-based) have been studied as heterogeneous [8] and homogeneous [9–11] catalysts to carry out the four electron oxidation of water to O_2 under photochemical conditions.

A possible way to measure the catalyst activity is by means of photoelectrochemical cells [12–14]. Alternatively, WO catalysts can be checked by the coupling with photosensitizers and sacrificial reagents [15–17]. This type of study is particularly suited to determine whether or not a given catalyst satisfies the kinetic and thermodynamic requirements for the water splitting reaction [16]. Very common is the use of a salt of tris(2,2′-bipyridyl)Ruthenium, $[Ru(bpy)_3]^{2+}$, in the presence of persulfate anions $S_2O_8^{2-}$) [8,18]. The photocatalytic cycle for such system is illustrated in Scheme 1 and consists of [19,20]: (a) visible light (λ = 450 nm) absorption by $[Ru(bpy)_3^{2+}]$ with formation of an excited state $[[Ru(bpy)_3^{2+,*}]]$; (b) oxidation of this latter species to $[Ru(bpy)_3^{3+}]$ by the persulfate, that is irreversible reduced (Eqs. (1) and (2)) and (c) in presence of the WO catalyst, the photosensitizer captures electrons from the catalyst surface, which in turn causes oxidation of water to O_2, while H^+ are produced (Eq. (3)). Without a WO catalyst, no O_2 is produced and the Ru^{3+} version of the photosensitizer rapidly decomposes due to OH^- attack on the bipyridile ring (Eq. (4)) [21], a reaction always competing with WO.

$$Ru(bpy)_3^{2+*} + S_2O_8^{2-} \rightarrow Ru(bpy)_3^{3+} + SO_4^{-2} + SO_4^{-\cdot} \quad (1)$$

$$Ru(bpy)_3^{2+} + SO_4^{-} \rightarrow Ru(bpy)_3^{3+} + SO_4^{-2} \quad (2)$$

$$4Ru(bpy)_3^{3+} + 2H_2O \xrightarrow{catalyst} 4Ru(pby)_3^{2+} + 4H^+ + O_2 \quad (3)$$

$$Ru(bpy)_3^{3+} + H_2O \rightarrow Ru(bpy)_3OH^{2+} + H^+ \rightarrow \text{decomposition products} \quad (4)$$

Closed batch reactors are generally used for WO studies, where O_2 evolution is analysed either by measuring O_2 dissolved in liquid with a Clark-type electrode [8,11] or measuring O_2 partial pressure in the gas headspace by Gas Chromatography (GC), assuming equilibrium between the gas and the liquid phases [6,19,20]. The initial rate of reaction is considered as the slope of the linear portion of the O_2 concentration curves obtained by the first method, whereas the total O_2 produced is determined from the GC-based type of measurement. From these, the initial Quantum Yield (or Turn Over Frequency) and the Turn Over Number of the catalyst, respectively, are determined, the most important variables to compare the performance of different catalysts.

We have undertaken recently a systematic study of Co-containing catalysts for WO, including Co-APO-5 zeotype [12,22], Co_3O_4 (this work) and, more recently, Co-MOFs [23]. As it concerns Co-APO-5, a first set of photoelectrochemical measurements was carried out, showing the occurrence of WO process [12]. As a second step, a flow reactor was set up, where oxygen evolution was followed in the gas phase: based on such measurements, preliminary kinetic features of a WO system similar to the one under study

(Co-APO-5 catalyst) were established by varying the catalyst mass, the persulfate loading and the dye concentration in the system. In this study, the assumption was made that, after an induction period, the rate of oxygen formation was constant in the first stages: this allowed to approximate the oxygen reaction rate by the slope of the oxygen evolution curve in the gas phase.

In the course of the work, it became clear that two improvements had to be made, namely the simultaneous measurement of oxygen evolution in the liquid phase, and the processing of data so to take into account mass transfer phenomena presumably distorting the reaction kinetics.

This is the subject of the present work, which reports a method, as a whole new, yielding the actual rate of oxygen production. Such a method features, on the one hand a bubbling reactor, where oxygen concentration is simultaneously measured in the liquid and in the gaseous phase, and, on the other hand, an appropriate mathematical model taking into account mass transfer phenomena occurring in the system.

To illustrate the data acquisition and processing, the method is applied to a set of measurements concerning the activity of a literature catalyst, Co_3O_4 supported on a mesoporous silica (MSU-H) [24], using the bubbling reactor in different operative conditions.

2. Experimental

2.1. Chemicals

All chemicals, *i.e.* silica MSU-H, $Co(NO_3)_2{\cdot}6H_2O$, $Ru(bpy)_3Cl_2{\cdot}6H_2O$ (99.95% trace metals basis), Na_2SO_4, $Na_2S_2O_8$, $Na_2HPO_4{\cdot}2H_2O$, NaH_2PO_4 H_2O, were from Sigma–Aldrich.

2.2. Materials

The nanostructured Co_3O_4 (a spinel, featuring both Co(II) and Co(III) ions) was supported on a commercial ordered mesoporous silica (MSU-H), by incipient wetness impregnation, according to a literature recipe [24]. An aqueous solution of $Co(NO_3)_2$ was used, in order to obtain a total Co loading of 4 wt%, followed by calcination at 380 °C under air flow. The so-obtained Co_3O_4/MSU-H material was checked by means of standard characterization techniques, including powders X-ray Diffraction (XRD), Field Emission-Scanning Electron Microscopy (FE-SEM), Energy Dispersive X-ray Analysis (EDX), Transmission Electron Microscopy (TEM) and N_2 adsorption/desorption isotherms at 77 K: the corresponding results are reported in the suplementary material (S.M.) in Figs. S1–S4.

2.3. The bubbling reactor system

Fig. 1 shows a picture of the reactor and the laboratory set-up: related technical drawings are reported in Fig. S5 (see S.M.). The quartz reactor has an internal diameter of 40 mm, a quartz window of 40 mm diameter on one side, and a total volume of 185 cm^3. An external jacket (4 mm thickness) is used to maintain the temperature constant by water flow. The cap, made in Teflon, warrants a hermetic closure of the system by means of O-rings. The cap has two holes, holding a InPro 6050/120 Clark-type sensor and an InPro 3250/120 electrode (both by Mettler Toledo) to measure oxygen concentration C_{O_2} [mg/l] and pH in the liquid phase, respectively.

In a typical experiment, the inert gas (argon) is injected into the liquid phase through a stainless steel tube of 1/16″ outside diameter (O.D.) placed in the centre of the cap. Outlet gases are recovered through a stainless steel tube of 1/8″ O.D., while temperature and pressure are measured by a type *K* thermocouple and a pressure transducer, connected to the reactor through a 1/8″ O.D. pipe. The sweeping gas inlet flow rate is controlled by a Bronkhorst® Mass Flow Controller. Pressure is controlled by the use of a Swagelok back pressure regulator. Pressure in reactor headspace, temperature, argon flow rate, pH and oxygen concentration in the liquid phase are constantly monitored, and data are collected by using a software developed in LabVIEW® platform. The oxygen volume fraction $p_{O_2,analyzer}$ (expressed in ppm) in the out-flowing gas is measured every minute through a micro Gas Chromatograph (Varian 490-μGC) equipped with a Molsieve 5A column of 10 m and a micro-TCD detector. The analysis method uses an injection time of 40 ms and the column temperature was maintained at 80 °C.

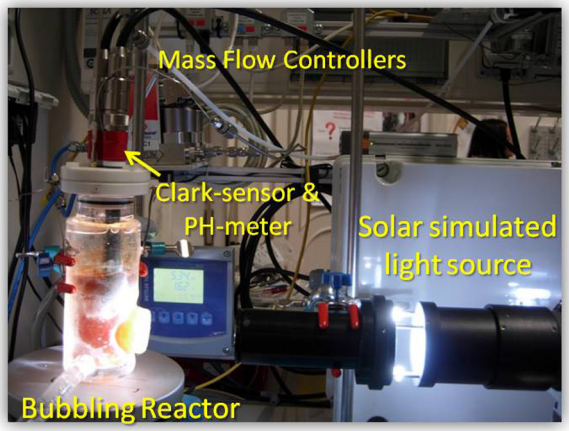

Fig. 1. Picture of the lab test-bench and the bubbling reactor for the photo-catalytic tests.

2.4. Photocatalytic WO experiments

In a typical experiment, the reaction mixture has the following constant composition: 40 mg Co_3O_4/MSU-H catalyst; 130 ml 0.05 M buffer phosphate (0.01 M NaH_2PO_4, 0.04 M Na_2HPO_4, with starting pH = 7.5); 150 mg Na_2SO_4; 100 mg $Na_2S_2O_8$ and 45 mg the $Ru^{2+}(bPy)_3$ Ruthenium complex. The pressure and the temperature were maintained constant at about 1.08 bar and 20 °C, respectively. The Buffer capacity ensured limited pH drop during the experiments (at most 0.5), actually found in unbuffered solutions due to the H^+ generation (as shown in Eq. (3)).

Prior to each measurement, Ar was flowed through the reactor in dark conditions until traces of O_2 and N_2 were no longer detected. Then, the reactor was illuminated through the quartz window with simulated solar light (100 mW/cm^2) by using a LIFI STA-40 model plasma lamp by Solaronix. Irradiance of incident light was measured with a Delta Ohm model HD2102.1 photo-radiometer. The complete spectrum of the lamp is reported in a previous paper [12]. The stirring rate was kept at 1100 rpm, to induce a turbulent motion of Ar bubbles through the suspension. The effect of Ar flux was studied at flow rates of 6, 12, 18 or 24 Nml/min, respectively, in different experiments.

A separate experiment was also run, with Ar flowing only through the gas-phase (at 6 Nml/min) and not in the stirred liquid, whereas in all the other experiments the reactor was in a bubbling configuration. This was performed in order to compare the results obtained by from a more conventional no bubbling case, respect to the bubbling reaction system.

3. Mathematical model

The starting experimental data are the values of the concentration of oxygen dissolved in the liquid C_{O_2} and the partial pressure of the gaseous oxygen at the reactor outlet $p_{O_2,analyzer}$. The constitu-

tive mass balances equations of the proposed pseudo-homogeneous model (solid phase is neglected) are:

- oxygen balance in the liquid phase:

$$(1-\varepsilon)V_R\dot{C}_{O_2} = k_L a \cdot \left(\frac{p_{O_2,b}}{H} - C_{O_2}\right) \cdot V_R + R_{O_2}(1-\varepsilon)V_R \quad (5)$$

- oxygen balance in the gaseous bubble phase:

$$\varepsilon V_R \frac{\dot{p}_{O_2,b}}{RT} = -k_L a \cdot \left(\frac{p_{O_2,b}}{H} - C_{O_2}\right) \cdot V_R - Q \cdot \frac{p_{O_2,b}}{RT} \quad (6)$$

- oxygen balance in the gas phase in the headspace above liquid:

$$V_g \frac{\dot{p}_{O_2}}{RT} = Q \cdot \left(\frac{p_{O_2,b}}{RT} - \frac{p_{O_2}}{RT}\right) \quad (7)$$

- oxygen balance in the gas phase at the analyzer:

$$p_{O_2,analyzer}(t) = p_{O_2}(t - \Delta t) \quad (8)$$

In Scheme 2 the mass transfer phenomena are illustrated taken into account in the mathematical analysis: the argon flow is injected into the liquid phase, and bubbles with a volume V_b are formed. These create a gas–liquid interface for the stripping of the oxygen being produced at the WO catalyst surface. The rate of oxygen production, denoted as R_{O_2}, is the rate of appearance of oxygen in the liquid phase, and lumps the actual reaction rate at the catalyst surface and the mass transfer of the oxygen from the catalyst surface to the bulk of the liquid. The model assumes that the reaction volume V_R, which is the sum of the liquid volume V_l and the gas bubble volume V_g, is homogeneously mixed, due to the intense stirring is provided to the system.

The rate of oxygen accumulation in the liquid phase is therefore due to the oxygen production rate R_{O_2} and to the rate of oxygen diffusion from the liquid phase, in which oxygen is present at concentration C_{O_2}, to the gas bubble phase, characterized by an oxygen partial pressure $p_{O2,b}$ (Eq. (5)).

The partial pressure of oxygen in the gas bubbles is increased by the same amount of oxygen left from the liquid (see Eq. (6)). The argon bubbles containing oxygen leave the liquid, and enter the gas headspace: the volume of the headspace V_g is considered as perfectly mixed, which is an acceptable condition at high gas flow rate, due to the turbulence it induces inside the gas headspace (Eq. (7)).

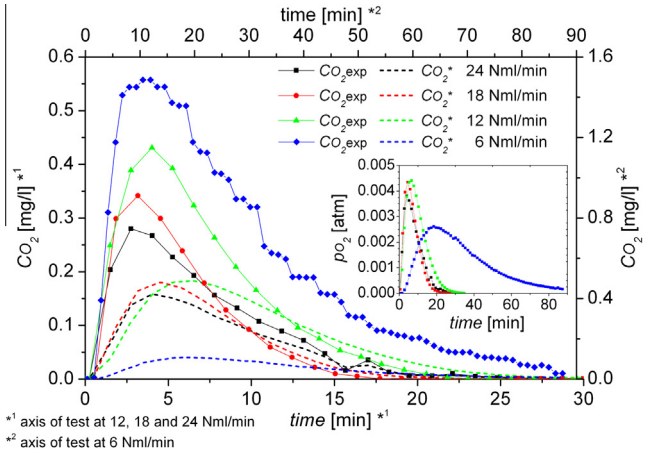

Fig. 3. Experimental data concerning the bubbling experiments performed at different stripping Ar flow rates. C_{O_2exp} and $p_{O_2,analyzer}$ (inset) as function of time (*line + symbols*) *and* calculated equilibrium data $C^*_{O_2}$ (dashed lines), at different stripping Ar flow rates.

Finally, Eq. (8)states that the partial pressure of oxygen measured at the GC analyzer is characterized by a lag time, during which the gas reaches the analyzer and a numerical response is obtained, which was measured experimentally.

From the above equations, it can be seen that, beside R_{O_2}, the only unknown parameter is the oxygen gas–liquid mass transfer resistance, given by the diffusion of the oxygen from the liquid bulk to the gas–liquid interface, and its further diffusion to the bulk of the gas phase. Under these conditions, the main resistance to the oxygen diffusion lies in the liquid phase, which is expressed by the parameter $k_L a$: this is the product of the mass transfer coefficient k_L, which depends on the system turbulence and, to a lesser extent, on the solid content in the liquid phase; and of the transfer area a, which is the result of the fluid-dynamics of the stirred liquid combined with the flow rate of the sweeping gas. The argon sweeping flow rate Q is approximated to be equal to the one at the outlet of

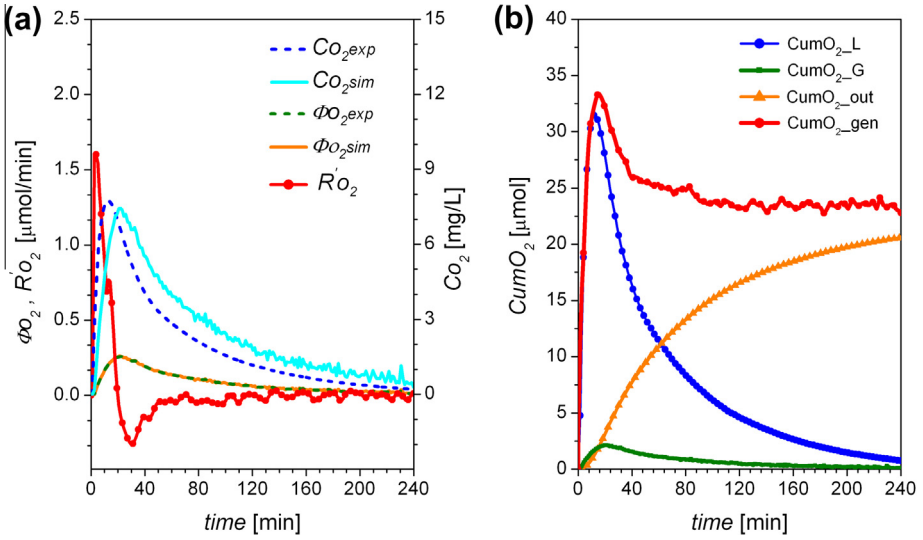

Fig. 2. Experimental and simulated data concerning a non-bubbling experiment. Section (a): time course of O_2 flow rate in the gas (Φ_{O_2exp}, Φ_{O_2sim}) O_2 concentration in the liquid phase (C_{O_2exp}, C_{O_2sim}) and derived reaction rate of O_2 generation referred to V_R (R'_{O_2}). Section (b): Cumulative oxygen ($CumO_2$), in all the environments of the reactor (_L: in the liquid phase; _*out*: flowed out to the GC analyzer; _*gen*: generated; _G: in the headspace above the liquid).

the reactor to the analyzer, because the stripped O_2 concentration during the test was always lower than 5×10^{-3} ppm.

A parameter entering calculations, which is to be known beforehand is the gas bubble volume fraction, ε, equal to V_b/V_R. The related value is roughly estimated through non-catalytic pure water bubbling tests, in which the average time of bubble upward flow is measured, and thus its residence time in the liquid is determined. Such a residence time, averaged among several samplings, is multiplied by the sweeping flow, in order to obtain the bubbles hold-up volume V_b. However, as later demonstrated numerically, it has a minor effect on the overall determination of k_La and R_{O_2}.

The solution of the set of equations (5–8) was analytically derived in order to understand the different time constants that contribute to the dynamics of the reactor. However, since the profile of R_{O_2} is not a priori known, a step-wise curve was adopted to simulate the ever-changing value of the reaction rate. As a result, as thoroughly reported in the Appendix B (see S.M.), the equation describing the evolution of $p_{O_2,analyzer}$ is:

where α and β are:

$$\alpha,\beta = \frac{-\left(\frac{k_La}{1-\varepsilon}+\frac{k_La}{\varepsilon}\cdot\frac{RT}{H}+\frac{Q}{\varepsilon V_R}\right) \pm \sqrt{\left(\frac{k_La}{1-\varepsilon}+\frac{k_La}{\varepsilon}\cdot\frac{RT}{H}+\frac{Q}{\varepsilon V_R}\right)^2 - 4\cdot\frac{Q}{\varepsilon V_R}\cdot\frac{k_La}{1-\varepsilon}}}{2} \tag{10}$$

From Eq. (9), it can be seen that three time constants characterize the dynamics of $p_{O_2,analyzer}$ to the light-induced oxygen production, namely: Q/V_g, α and β. The last two constants are negative, with β being far greater in absolute terms, and they depend upon only two unknown constants: k_La and ε. However, ε has little influence in practical terms, being the values it possibly assumes in the tests of the order of 10^{-3}. This will be more clearly shown below, when numerical details of Q/V_g, α and β are discussed. It can be understood, however, by the evidence that $p_{O_2,analyzer}$ depends on the mean residence times in the liquid volume V_l, equal to $(1-\varepsilon)\cdot V_R$, in the gaseous bubble volume V_b, equal to $\varepsilon\cdot V_R$, and in the headspace

$$p_{O_2,analyzer} = \frac{(1-\varepsilon)V_R\cdot RT}{Q}\cdot\sum_{i=1}^{N} R_{O_2,i-1}\cdot\left\{\begin{array}{l}\left[\begin{array}{l}\left(1-e^{-\frac{Q}{V_g}(t-b_{i-1}-\Delta t)}\right)+\frac{\beta}{\alpha-\beta}\cdot\frac{\frac{Q}{V_g}}{\alpha+\frac{Q}{V_g}}\cdot\left(e^{\alpha\cdot(t-b_{i-1})}-e^{-\frac{Q}{V_g}(t-b_{i-1}-\Delta t)}\right)+\\ -\frac{\alpha}{\alpha-\beta}\cdot\frac{\frac{Q}{V_g}}{\beta+\frac{Q}{V_g}}\cdot\left(e^{\beta\cdot(t-b_{i-1})}-e^{-\frac{Q}{V_g}(t-b_{i-1})}\right)\end{array}\right]\cdot u(t-b_{i-1}-\Delta t)+\\ -\left[\begin{array}{l}\left(1-e^{-\frac{Q}{V_g}(t-b_i-\Delta t)}\right)+\frac{\beta}{\alpha-\beta}\cdot\frac{\frac{Q}{V_g}}{\alpha+\frac{Q}{V_g}}\cdot\left(e^{\alpha\cdot(t-b_i)}-e^{-\frac{Q}{V_g}(t-b_i-\Delta t)}\right)+\\ -\frac{\alpha}{\alpha-\beta}\cdot\frac{\frac{Q}{V_g}}{\beta+\frac{Q}{V_g}}\cdot\left(e^{\beta\cdot(t-b_i)}-e^{-\frac{Q}{V_g}(t-b_i-\Delta t)}\right)\end{array}\right]\cdot u(t-b_i-\Delta t)\end{array}\right\} \tag{9}$$

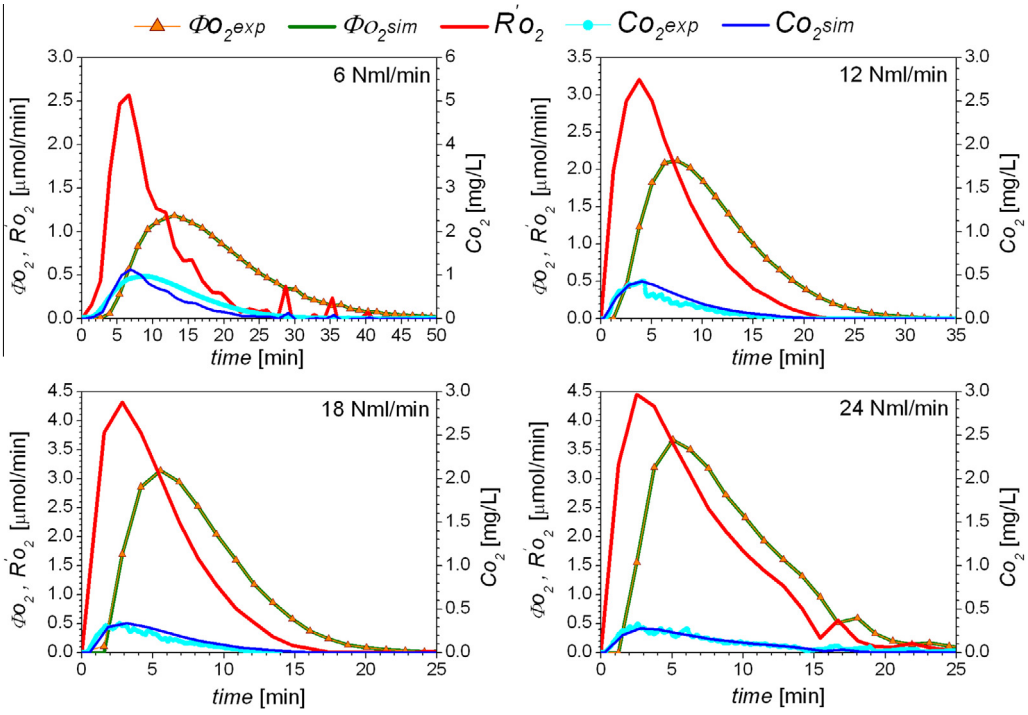

Fig. 4. Effect of bubbling flow rate on the time course of O_2 evolution (experimental and simulated data) and calculated reaction rate. Φ_{O_2}: O_2 flow rate in the gas phase; C_{O_2}: O_2 concentration in the liquid phase ($_{exp}$: experimental data; $_{sim}$: simulated data). R'_{O_2}: simulated reaction rate of O_2 generation referred to V_R. Water oxidation tests with 40 mg of Co_3O_4/MSU-H.

volume V_g. Since $\varepsilon \cdot V_R$ is negligible as compared to the other volumes, the residence time of the oxygen in this volume is far below the one in the other environments. In fact, only β is considerably affected by the value of ε:

$$\beta \approx -\left(\frac{k_L a}{\varepsilon}\cdot\frac{RT}{H}+\frac{Q}{\varepsilon V_R}\right) \tag{11}$$

since the second term under the square root is negligible as compared to the first one, and $k_L a/(1-\varepsilon)$ vanishes with respect to the other two addends containing ε (see Eq. (10)), as can be later verified numerically, given the values assumed by $k_L a$, ε, Q and V_R.

On the other hand, α is sensitive to it only for $\varepsilon > 0.01$, which is never reached in our practical experimental conditions. In fact α is:

$$\alpha = \frac{\alpha\beta}{\beta} \approx \frac{\frac{k_L a}{1-\varepsilon}\cdot\frac{Q}{\varepsilon V_R}}{-\left(\frac{k_L a}{\varepsilon}\cdot\frac{RT}{H}+\frac{Q}{\varepsilon V_R}\right)} \approx -\frac{1}{\frac{RT}{H}\cdot\frac{(1-\varepsilon)V_R}{Q}+\frac{1-\varepsilon}{k_L a}} \approx -\frac{1}{\frac{RT}{H}\cdot\frac{V_R}{Q}+\frac{1}{k_L a}} \tag{12}$$

As a result, the coefficient of the exponential term containing α as exponent in Eq. (9) is practically not dependant on ε, because:

$$\frac{\beta}{\alpha-\beta} \approx -1 \tag{13}$$

while the one with β as exponent is almost negligible for the system dynamics, because of its instantaneous decay. This behavior indeed reflects the very low residence time of the oxygen in the gaseous bubble immerged in the liquid, with respect to the residence time in the liquid itself or in the gas headspace of the reactor.

The procedure to numerically derive the rate of oxygen production due to light-induced water oxidation is depicted in the Scheme 3, which reads as follows: after assuming an initial guess value for $k_L a^{(0)}$, Eq. (9) is used to calculate the value of $p_{O_2,analyzer}$ by fitting the experimental data from the GC analyzer; b_i corresponds to each sampling time, while Δt is the time delay elapsed for each measurement of the gas-chromatograph (estimated at 60s from calibration); consequently, the oxygen generation is computed at each experimental point, being equal to $R^{(0)}_{O_2}$.

The next step is the verification of the $k_L a^{(0)}$ assumed for the $R^{(0)}_{O_2}$ curve determination: the oxygen concentration in the liquid is calculated as follows (see Eq. A17 in the Appendix B):

$$C_{O_2,i} = R_{O_2,i}\cdot\left[\begin{array}{c}\left(\frac{(1-\varepsilon)V_R}{\varepsilon Q}\cdot\frac{RT}{H}+\frac{1-\varepsilon}{k_L a}\right)+\frac{1}{\alpha-\beta}\cdot\left(1+\frac{\frac{k_L a}{\varepsilon}\frac{RT}{H}+\frac{Q}{\varepsilon V_R}}{\alpha}\right)\cdot e^{\alpha\cdot t}+\\ -\frac{1}{\alpha-\beta}\cdot\left(1+\frac{\frac{k_L a}{\varepsilon}\frac{RT}{H}+\frac{Q}{\varepsilon V_R}}{\beta}\right)\cdot e^{\beta\cdot t}\end{array}\right] \tag{14}$$

and compared to its experimental value. The least square difference between the computed and the experimental curves is used to update the value of $k_L a^{(0)}$ to $k_L a^{(1)}$. An iterative process yields the best set of $k_L a^{(n)}$ and $R^{(n)}_{O_2}$ in 2–3 iterative steps. The "ease" of the iterative step depends on the value of Q: if its value is high enough to speed-up the stripping in the liquid, then both constants α and β are great enough to make their exponential terms fade faster than the one ascribed to the gas phase Q/V_g, as will be later shown with practical experimental data. In this case, $p_{O_2,analyzer}$ and C_{O_2} are much less interrelated and can be computed almost within 1 iteration. Conversely, if the value of Q is low, the stripping procedure is quite slow and α causes slower exponential decay, which influences the whole system dynamics. These aspects of the system dynamics were specifically modeled and studied with the intent to understand which resistance is dominant in the oxygen output, and which testing conditions can maximize the oxygen production rate and the total oxygen output obtained with a water-splitting catalytic system.

Modeling with no bubbling of gas in the liquid was also considered in order to derive the oxygen production rate for this case (see Section 4.1). It is worth noticing that, in this case, $k_L a$ assumes the meaning of the oxygen mass transfer resistance from the liquid bulk to the gas–liquid interface, i.e. the liquid surface itself. The full set of equation are included in the Appendix B, from Eqs. A25–A29.

4. Results and discussion

4.1. Non-bubbling WO experiment

The non-bubbling experiment is reported in Fig. 2. Section (a) reports the time course of the concentration of oxygen dissolved in the liquid ($C_{O_2 exp}$), and the flow rate of oxygen at the GC analyzer ($\Phi_{O_2 exp}$) calculated as:

$$\Phi_{O_2\,exp} = p_{O_2,analyzer}\cdot\frac{Q}{RT} \tag{15}$$

The corresponding simulated curves $C_{O_2 sim}$, $\Phi_{O_2 sim}$ and the rate of appearance of oxygen in the liquid phase R_{O_2} versus time were calculated using Eqs. A27 and A28 (as explained in Section 3) and are represented in the same figure. Section (b) of Fig. 2 reports the related integral values, measured in μmols of oxygen.

The curve of $C_{O_2 exp}$ exhibits a very sharp peak, due to the fact the almost no removal of oxygen occurs. The dynamic of oxygen accumulation in the liquid phase during the first 30 min of test is therefore very fast, as a consequence of the absence of bubbling. $C_{O_2 exp}$ evidences a delay respect to $C_{O_2 exp}$ due to the fact that the model assumes that the gas in the headspace of the reactor is homogeneous and completely mixed. When no bubbling is applied, such hypothesis decays because the lower turbulence in the system generates a gradient of concentration between the liquid surface and the outlet gas. Thus, such assumption, initially considered for the bubbling condition, is used in this case just as a good approximation for comparison purposes. On the other hand, the time course of $\Phi_{O_2 sim}$ fits very well the experimental data in the gas phase, that is important since the reaction rate is calculated starting from this value (as can be seen form Scheme 3).

It is worth of note that the amount of oxygen collected at the end of experiment from the outlet gas phase ($CumO_2$_out) is less than that generated at a given moment in the liquid media ($CumO_2$_gen), which is evidence of some oxygen consumption with a negative rate of reaction (R'_{O_2}) after 20 min of test. A most likely reason is the oxidative degradation of the sensitizer that takes place in this kind of experiments [21]. Moreover, O_2 was not totally stripped from the liquid even after 240 min of test, as can be seen from the cumulative curve: $CumO_2$_L. Indeed, under no bubbling conditions, the mass transfer coefficient $k_L a$ (estimated to be 1.45×10^{-4}) is very low in comparison with a bubbling situation (as explained later in Section 4.3). Therefore,

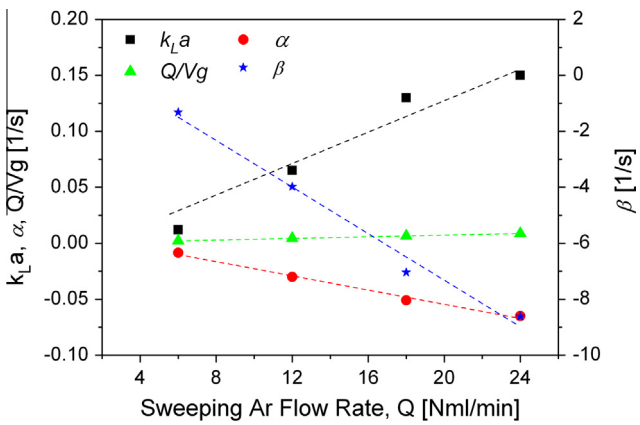

Fig. 5. Plot of $k_L a$ against stripping gas flow at constant stirring rate of 1100 rpm.

under no bubbling conditions, the high mass transfer resistance for the stripping of the O_2 from the liquid bulk to the liquid surface, arises to underestimations in the total amount of oxygen evolved when it is measured in the gas phase, as commonly made in the literature [19,20].

Besides the possibility to obtain reliable kinetic data, which is the explicit goal of this paper, an efficient removal of oxygen from the liquid phase is desirable also to avoid this latter unwanted phenomenon.

4.2. Bubbling WO experiments and rate of O_2 production

An important point in WO experiments is whether the gas phase and the liquid phase are at equilibrium, as far as partition of O_2 is concerned, as often assumed in approximate treatments in the literature [6,19,20].

Fig. 3 compares the curves observed of C_{O_2}, and the values of $C^*_{O_2}$, the concentration of oxygen dissolved in the liquid at equilibrium with $p_{O_2,analyzer}$ (Fig. 3-inset graph) as coming from application of Henry's law. It is worth mentioning that the curves at 6 Nml/min are referred to the top x axis and left y axis of Fig. 3.

It results that the concentration of oxygen in the liquid is higher than it would occur if diffusional limitation to its stripping were not present. Therefore, the sampling of the gas phase alone is not representative of the real reaction rate in the liquid, which could lead to its underestimation; conversely, in a closed reactor without any stripping of the produced oxygen, parasitic reaction involving oxygen consumption cannot be avoided, as shown in Section 4.1.

Such observation affords importance to the testing procedure presented in the present paper, where no equilibrium is assumed, and, through a mathematical modeling of the system, the real reaction rate of oxygen production at each moment of the test is arrived at.

The raw data concerning bubbling experiments at different Ar flow rates are shown in Fig. 4, where $C_{O_2 exp}$ and $\Phi_{O_2 exp}$ have the same meaning as above. As a result of the above mathematical treatment, the corresponding simulated curves $C_{O_2 sim}$, $\Phi_{O_2 sim}$ and the rate of appearance of oxygen in the liquid phase R_{O_2} versus time were calculated and represented in the same figure.

As a general feature of all plots in Fig. 4, one can see that $C_{O_2}(t)$ shows a steady growth, followed by a decrease; $\Phi_{O_2 2(t)}$, which is proportional to the partial pressure of oxygen in the analyzer $p_{O_2,analyzer}$ (see Eq. (15)), features an induction period, then a nearly linear portion followed by a maximum and a quasi-exponential decay. Such behavior is expected in this type of photo-catalytic systems due to the consumption of the sacrificial reactant and competing side reactions that cause the degradation of the photosensitizer (see Scheme 1 and Introduction).

A time lag of ca. 1 min occurs between the measurement of the concentration in the liquid phase and that in the gas phase, due to the time needed for the gas to move from the reaction chamber to the analyzer. This was taken into account in Eq. (8).

In contrast, R_{O_2} shows no or negligible induction time, especially at high stripping flow rates: its value increases quickly from $t = 0$ till a maximum value, then it decreases quasi-exponentially in the same way as Φ_{O_2}.

The presence of a maximum requires some comments, as, from a general point of view, if only the sacrificial reactant concentration impacts on the pathway from the water to oxygen formation, R_{O_2} should be maximum at $t = 0$. Indeed, such a behavior was observed when testing semiconductor materials, suspended in a solution of a sacrificial reactant, for the photo-catalytic WO reaction, in the absence of the Ru sensitizer. This is the case with commercial tungsten oxide (WO_3) reported in the S.M. (Fig. S6).

The maximum at $t > 0$ represents the dynamics of the system when the Ru sensitizer is present, and was also evidenced in the test performed without bubbling (Fig. 2), in which the onset of the reaction does not start instantaneously after illumination. Such lag time is due to the reaction mechanism, because, on the one hand, the sensitizer has to be oxidized from Ru(II) to Ru(III); on the other hand, Ru(III) is subjected to both reduction back to Ru(II) and degradation reactions. We have observed the same dynamics

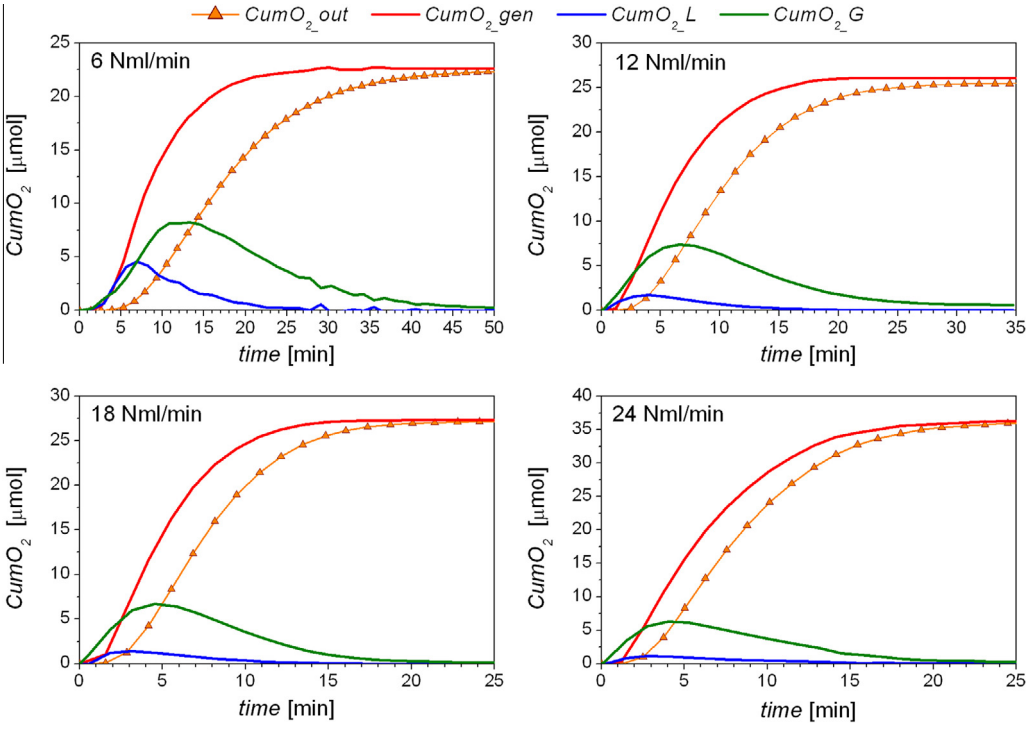

Fig. 6. Time course of cumulative oxygen ($CumO_2$), in all the environments of the reactor (_L: in the liquid phase; _out: flowed out to the GC analyzer; _gen: generated; _G: in the headspace above the liquid) at four different Ar bubbling flow rates. Water oxidation tests with 40 mg of Co_3O_4/MSU-H.

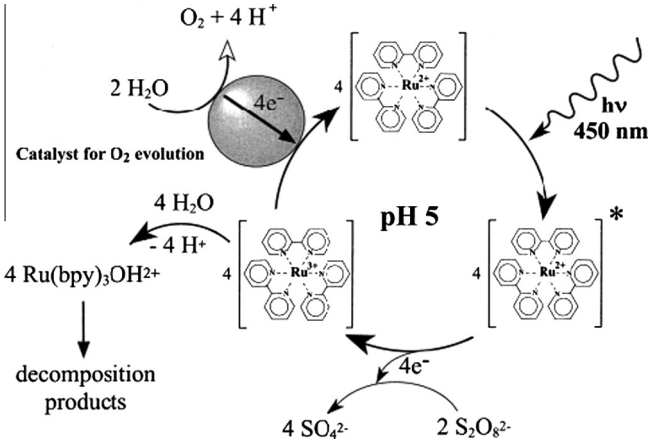

Scheme 1. Schematic of the photocatalytic oxidation of water by the $[Ru(bpy)_3]^{2+}$-catalyst system, showing the competing decomposition reaction of the oxidized sensitizer. Reproduced from [24].

in a former work of our group [22], in which the kinetics of the WO reaction using a Co-APO-5 catalyst was analyzed in the presence of $Ru^{2+}(bPy)_3$ complex. This behavior is difficult to be observed when completely closed reactors are used (as happens in most works in the literature), since in such case it can be measured only the cumulative O_2 concentration and, thus the reaction rate is assumed to be constant at the beginning of the test.

4.3. Fitting of experimental data and mass transfer coefficient (k_La)

For the calculation of $\Phi_{O_2 sim}$, the simulated $p_{O_2,analyzer}$ is used. $\Phi_{O_2 exp}$ and $\Phi_{O_2 sim}$ perfectly overlap in all cases, since the latter is obtained from point-to -point fitting, whereas $C_{O_2 sim}$ approaches the profile of $C_{O_2 exp}$ as a result of the choice of a specific k_La (Scheme 3). In general, the analysis of O_2 in gas phase was more stable with respect to the measurement in the liquid, that is influenced by the mixing of the solution, and was therefore selected as the source for the fitting procedure leading to R_{O_2} determination. In fact, in some cases, it is observed that a sudden decrease on the liquid O_2 concentration occurs due to stirring instabilities.

Even if the profiles of C_{O_2} and Φ_{O_2} in Fig. 4 are similar with all investigated stripping flow rates, important differences are noted as far as the extent of production is concerned: the increase of the bubbling flow rate reduces the lag time to the minimum, as can be noticed by the fact that the maximum of the oxygen production rate in the volume V_R (R'_{O_2}) occurs after 91 s at 24 Nml/min, after 111 s at 18 Nml/min, after 165 s at 12 Nml/min, after 340 s at 6 Nml/min. Moreover, peak values equal to 2.57, 3.21, 4.32 and 4.45 μmol/min were obtained for 6, 12, 18 and 24 Nml/min, respectively. A plateau seems to be reached, and 24 Nml/min appears to be a suitable operating condition.

Two possible interpretations are possible for the increase of oxygen yield with the bubbling flow rate. On the one hand, it may occur that the faster the removal of oxygen from the liquid, the higher the rate of WO reaction, because oxygen inhibits the reaction itself (e.g. by oxidizing the Ru complex or by adsorption on the catalyst). On the other hand, bubbling is effective in decreasing the diffusional limitations to the various steps of reaction (Scheme 1), so increasing the rate of WO. This is proven by the much lower peak value of R'_{O_2}) reached in the case with no bubbling in the liquid phase, which was equal to 1.6 (see Fig. 2-a), 0.6 times the one in the case of bubbling at analogous flow rate. In fact, in such a case the k_La obtained (1.45×10^{-4}) was 2/3 orders of magnitude lower than the obtained values with bubbling in the reaction system (see Fig. 5).

The computation of R'_{O_2}) showed that its profile was much different from the one of the O_2 flow rate at the analyzer ($\Phi_{O_2 exp}$), both in terms of the maximum value of R'_{O_2}) and of the time at which this maximum was located. This difference was more and more evident at decreasing stripping flow rates, because of a poorer stripping in these conditions (as appreciable by the higher value of $C_{O_2 exp}$ at low flow rates) and longer residence time of the oxygen in the liquid which delays its appearance at the GC.

In these cases, the assumption of $\Phi_{O_2 exp}$'s maximum as an approximation of the highest water splitting activity of the catalyst might be severely erroneous when low sweeping flow rates are used, but at high stripping velocities it could be considered a priori as a conservative underestimation of the maximum catalyst activity. In fact, the peak of $\Phi_{O_2 exp}$ was always lower than the one of R'_{O_2}, with a difference of 54%, 34%, 27% and 18%, for the tests at 6, 12, 18 and 24 Nml/min, respectively.

However, also the time at which the maximum catalyst activity occurs could be considerably shifted with respect to the one of $\Phi_{O_2 2 exp}$. An indication of the time at which the powder catalyst shows the maximum activity can be seen, apart from the R'_{O_2} peak itself, by the $C_{O_2 exp}$ and $C_{O_2 sim}$ curves, which share the same maximum in all tests: it is worth underlining that, once fitted the $\Phi_{O_2 sim}$ to the $\Phi_{O_2 exp}$, the parameter k_La cannot shift the maximum of $C_{O_2 sim}$ versus time, and its occurrence at the very same time of $C_{O_2 exp}$ is not the result of any adjustment of the fitting procedure.

This analysis indicates that appropriate testing conditions should be devised in order to know the potential of a water-splitting

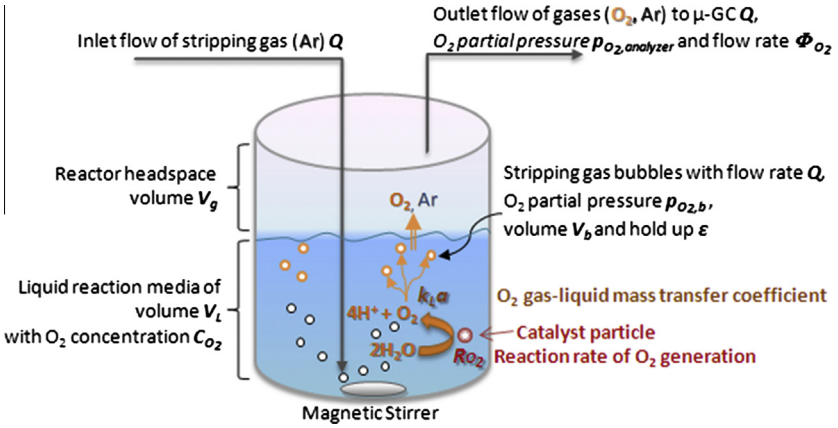

Scheme 2. Representation of mass transfer phenomena occurring in the reaction system.

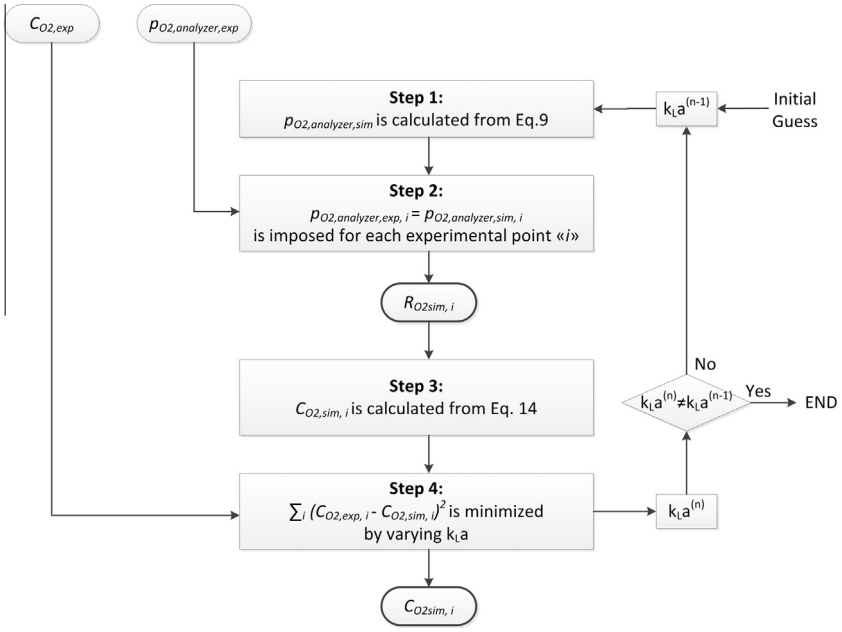

Scheme 3. Flow diagram for the resolution of mass transfer equations and calculation of R_{O_2} and k_La from experimental data.

catalyst, and these conditions are strictly linked to the activity of the catalyst itself; in fact, in the occurrence of catalysts exhibiting higher reaction rates, 24 Nml/min might be too low to approach its plateau. Conversely, when the kinetics of the reaction is slower such as in the case of the WO_3 semiconductor, reported in the S.M. (Fig. S6-a), the proper value of sweeping flow rate should be found in order to maintain high the sensibility of the analytical instruments (μ-GC and Clark type electrode) by avoiding a too high dilution of the oxygen in the liquid and gas phases. In that case, the use of high stirring velocity is fundamental to further reduce the resistance due to mass transfer phenomena.

The full set of k_La values calculated for the four sweeping flows, along with the values of α, β (for $\varepsilon = 0.001$) and Q/V_g are reported in Fig. 5 and Table S1 (see S.I.). It appears that β is always two orders of magnitude greater than α in absolute terms, and thus its exponential decay is much faster than the one of α. Experimental values of k_La are within the range commonly encountered when empirical correlations are used [25,26], for these specific stirring velocities. The proportionality of α and β to k_La is ascribable to their formulation, written in Eq. (10).

The reported data allows anyway a check of the efficiency of the model. Under the reasonable assumption that stripping gas flows, differing by less than one order of magnitude, correspond to the same type of gas bubbles, i.e. to the same average size, it results that the surface exposed a is proportional to the volume flown per unit time. The parameter k_La is thus expected to be proportional to the stripping gas flow: Fig. 5 shows that it is indeed so.

In addition, the agreement between the simulated and experimental curve of the oxygen concentration in the liquid, obtained through the calculation of k_La by the least squares difference method, led to the following coefficient of determination R^2: 0.93 for 6 Nml/min, 0.92 for 12 Nml/min, 0.95 for 18 Nml/min, 0.96 for 24 Nml/min; with a confidence interval for k_La, α and β within ±6% of values represented in Fig. 5, for all the considered stripping flow rates (see Table S1). These values show that the accuracy of the proposed method is generally satisfactory, and it increases at increasing flow rates, i.e. the accuracy of k_La estimation becomes less critical when the difference between the actual and equilibrium concentration of oxygen in the liquid decreases.

4.4. Catalyst activity versus sweeping flow rate

Fig. 6 shows the cumulative oxygen ($CumO_2$) versus time, for all configurations of the reactor used. Curves of O_2 in liquid phase ($CumO_2\_L$) and O_2 flowed out to the GC analyzer ($CumO_2\_out$) were obtained from experimental data, whilst the cumulative O_2 generated ($CumO_2\_gen$) was determined from the calculated O_2 generation rate (R_{O_2}), by integration of its curves in Fig. 4. Cumulative O_2 in the headspace of the reactor ($CumO_2\_G$) was calculated the profile of p_{O2}. Clearly, the sum and $CumO_2\_out + CumO_2\_L + CumO_2\_G$ equals $CumO_2\_gen$ at any time, since each generated oxygen molecule can be either located in the liquid, or in the gas headspace above the liquid, or is already flowed through the analyzer.

The profile of $CumO_2\_gen$ is remarkably sensitive to $CumO_2\_L$ only the initial part of the test, and just at the lowest stripping flow rate (6 Nml/min), in which the disengagement of the oxygen is not rapid; in this case, the time constant α is quite low, and the corresponding exponential decay is slow. Subsequently, the oxygen accumulates prevalently in the gas headspace.

In all other cases, the oxygen is mainly located in the gas headspace (from 12 to 24 Nml/min), as can be seen from the $CumO_2\_G$ curve, while $CumO_2\_L$ is much less relevant than for 6 Nml/min, reflecting the fact that the time constant Q/V_g is much lower than α.

With increasing Q/V_g values, the amounts of oxygen in the liquid and in the headspace are progressively reduced, and the difference between $CumO_2\_gen$ and $CumO_2\_out$ is also decreased, as already observed in the derivative curves of Fig. 6.

Another important outcome is that the peaks of R'_{O_2} not only assume increasing values at higher stripping flow rates, but the total O_2 evolved is also affected: $CumO_2\_G$ reaches 36.87 μmol at 24 Nml/min, while constantly decreasing values were observed at all lower sweeping flows. We believe that, due to the higher accumulation of O_2 into the reaction media at lower sweeping Ar flow rates, the reaction starts to be controlled by the mass transfer, i.e. the diffusion of O_2 from catalyst surface to the liquid media, while the solution becomes saturated by the O_2 produced, that is supported by the lower reaction rates obtained at lower Ar flow rates (as described in Section 4.2). In contrast, at higher stripping flow rates, the reaction is not inhibited by the O_2 dissolved in the liquid

media and thus the reaction is no more controlled by the diffusion, if not by the kinetics of water oxidation on the surface of the catalyst. Therefore, in such conditions, it is possible to more accurately measure the real kinetics of the catalyst under study, and its actual maximum reaction rate for water oxidation. Moreover, since in a real system the product will be continuously removed from the reaction media, we can state that the use of this bubbling reaction system is a reliable way to screen the activity of different catalyst materials for the photo-activated water-splitting reaction.

5. Conclusions

The method proposed appears to be reliable in determining both the total amount of oxygen produced, and the rate of oxygen evolution as a function of time, the latter a feature not readily measurable in batch reactors. The oxygen production rate was observed to progressively raise with increasing argon flow rate up to a plateau value. Such results suggest that the reaction is inhibited by the presence of O_2 in the solution, whereas its rapid removal increases the rate of reaction, so enhancing also the total amount of O_2 produced. Moreover, the time needed to observe the complete dynamic of the reaction system is reduced of 80–90% between the non-bubbling test and the bubbling condition.

Internal checks of the procedure are, on the one hand, the observed proportionality of the parameter k_L a with stripping gas flow, a condition not imposed by the model. On the other hand, the observation that, with high stirring and flow rates, the cumulative amount of oxygen measured at the end of the experiment coincides with that computed from the integration of the calculated reaction rate.

Finally, the features of $R'_{O_2}(t)$ are in qualitative agreement with the reaction cycle in Scheme 1, provided that both formation and depletion (via two paths) of the $Ru(biPy)_3^{3+}$ complex in the cycle are slow (rate-determining) steps with respect to all others, including WO by the Co^{3+} active species. In this way, the initial nearly linear slope is explained, as well as the maximum and the quasi-exponential decrease at the end of reaction. Future work will deal with the quantitative interpretation of the $R_{O_2}(t)$ curves.

In a previous work [22], based only on the gas phase data, kinetic considerations have been made by assuming that, after an initial delay, the rate of reaction is constant for about 15 min. By using the new methodology to compute the values of $R'_{O_2}(t)$, a more accurate set of data is now available for the derivation of kinetic data, finalized to understand the WO reaction mechanisms.

Acknowledgments

Authors thanks Diego Manfredi and Carminna Ottone for their support on FE-SEM measurements and testing of the semiconductor material. Massimiliano Anastasi, Marco Mori and Jubal Gil Vivas from HYSYTECH s.r.l. are acknowledged for the technical support in the elaboration of the reactor drawings, the lab test-bench and the acquisition software in LabView®. The European commission is gratefully acknowledged for the financial support for this work, which is a part of the 7th Framework Programme: Energy-2008-FET Project Solhydromics nr. 227192 and NMP-2012 Project ECO^{2}CO$_2$ nr.309701.

Appendices A and B. Supplementary material

Supplementary data associated with this article can be found, in the online version, at http://dx.doi.org/10.1016/j.cej.2013.08.094. Results of chemical and morphological characterization of the Co_3O_4/MSU-H material (XRD pattern, BET, pore size distribution, FE-SEM micrograph, EDX micro-analysis data and TEM analysis), technical drawings of the bubbling reactor, and data concerning the test of commercial WO_3, are reported in the supplementary data in the Appendices A and B. The Appendix B describes the analytical solution of mass balance equations and the derivation of equations (9) to (14).

References

[1] M. Grätzel, Photoelectrochemical cells, Nature 414 (2001) 338–344.
[2] W.J. Youngblood, S.-H.A. Lee, K. Maeda, T. Mallouk, Visible light splitting using dye-sensitized oxide semiconductors, Acc. Chem. Res. 42 (12) (2009) 1966–1973.
[3] S. Bensaid, G. Centi, E. Garrone, S. Perathoner, G. Saracco, Toward artificial leaves from solar hydrogen and fuels from carbon dioxide, ChemSusChem 5 (2012) 500–521.
[4] A. Fujishima, K. Honda, Electrochemical photolysis of water at a semiconductor electrode, Nature 238 (5358) (1972) 37–38.
[5] T. Bak, J. Nowotny, M. Rekas, C.C. Sorrell, Photo-electrochemical hydrogen generation from water using solar energy. Materials-related aspects, Int. J. Hydrogen Energy 27 (2002) 991–1022.
[6] A. Kudo, Y. Miseki, Heterogeneous photocatalyst materials for water splitting, Chem. Soc. Rev. 38 (2009) 253–278.
[7] D. Gust, T.A. Moore, A.L. Moore, Solar fuels via artificial photosynthesis, Acc. Chem. Res. 42 (12) (2009) 1890–1898.
[8] A. Harriman, I.J. Pickering, J.M. Thomas, P.A. Christensen, Metal oxides as heterogeneous catalysts for oxygen evolution under photochemical conditions, J. Chem. Soc. Faraday Trans. I 84 (8) (1988) 2795–2806.
[9] Z. Huang, Z. Luo, Y.V. Geletii, J.W. Vickers, Q. Yin, D. Wu, Y. Hou, Y. Ding, J. Song, D.G. Musaev, C.L. Hill, T. Lian, Efficient light-driven carbon-free cobalt-based molecular catalyst for water oxidation, J. Am. Chem. Soc. 133 (2011) 2068–2071.
[10] Y.V. Geletii, B. Botar, P. Kögerler, D.A. Hillesheim, D.G. Musaev, C.L. Hill, An all-inorganic, stable, and highly active tetraruthenium homogeneous catalyst for water oxidation, Angew. Chem. Int. Ed. 47 (2008) 3896–3899.
[11] L. Duan, Y. Xu, P. Zhang, M. Wang, L. Sun, Visible light-driven water oxidation by a molecular ruthenium catalyst in homogeneous system, Inorg. Chem. 49 (2010) 209–215.
[12] S. Zanarini, S. Vankova, S. Hernandez, V.S. Ijeri, M. Armandi, E. Garrone, B. Bonelli, B. Onida, P. Spinelli, CoAPO5 as a water oxidation catalyst and a light sensitizer, Chem. Commun. 48 (2012) 5754–5756.
[13] Y. Surendranath, M.W. Kanan, D.G. Nocera, Mechanistic studies of the oxygen evolution reaction by a cobalt-phosphate catalyst at neutral pH, J. Am. Chem. Soc. 132 (46) (2010) 16501.
[14] K. Sivula, F. Le Formal, M. Gratzel, Solar water splitting: progress using hematite (α-Fe_2O_3) photoelectrodes, ChemSusChem 4 (2011) 432–449.
[15] V. Artero, M. Chavarot-Kerlidou, M. Fontecave, Angew. Chem. Int. 50 (2011) 2–31.
[16] R.M. Navarro, M.C. Alvarez-Galvan, F. del Valle, J.A. Villoria de la Mano, Jose L.G. Fierro, Water splitting on semiconductor catalysts under visible-light irradiation, ChemSusChem 2 (2009) 1–16.
[17] M.M. Najafpour, F. Rahimi, E.M. Aro, C.-H. Lee, S.I. Allakhverdie, Nano-sized manganese oxides as biomimetic catalysts for water oxidation in artificial photosynthesis: a review, J. R. Soc. Interface 9 (2012) 2383–2395.
[18] J. Kiwi, M. Gratzel, Hydrogen evolution from water induced by visible light mediated by redox catalysis, Nature 285 (1979) 657.
[19] M. Hara, J.T. Lean, T.E. Mallouk, Photocatalytic oxidation of water by silica-supported tris(4,4¢-dialkyl-2,2¢-bipyridyl)ruthenium polymeric sensitizers and colloidal iridium oxide, Chem. Mater. 1 (2001) 4668–4675.
[20] M. Hara, C.C. Waraksa, J.T. Lean, B.A. Lewis, T.E. Mallouk, Photocatalytic water oxidation in a buffered Tris(2,2¢-bipyridyl)ruthenium complex-colloidal IR_{O_2} system, J. Phys. Chem. A 104 (2000) 5275–5280.
[21] P.K. Ghosh, B.S. Brunschwig, M. Chou, C. Creutz, N. Sutin, Thermal and light-induced reduction of the ruthenium complex cation $Ru(bpy)_3^{3+}$ in aqueous solution, J. Am. Chem. Soc. 106 (17) (1984) 4772–4783.
[22] M. Armandi, S. Hernandez, S. Vankova, S. Zanarini, B. Bonelli, E. Garrone, Visible-light driven oxidation of water as catalyzed by Co-APO5 in the presence of Ru sensitizer, ACS Catal. 3 (2013) 1272–1278.
[23] S. Vankova, C. Pagliano, E. Celasco, M. Thalluri, S. Hernandez, D. Hidalgo, G. Saracco, B. Onida, J. Barber, Metal-organic frameworks as water splitting photocatalysts, 15th International Congress on Catalysis, Munich, Germany, poster, program, July 1–6 2012, pp. 48.
[24] F. Jiao, H. Frei, Nanostructured cobalt oxide clusters in mesoporous silica as efficient oxygen-evolving catalysts, Angew. Chem. 121 (2009) 1873–1876.
[25] W.T. Koetsier, D. Thoenes, J.F. Frakena, Mass transfer in a closed stirred gas/liquid contactor. Part 1: the mass transfer rate k_LS, Chem. Eng. J. 5 (1973) 61–69.
[26] L.A. Tribe, C.L. Briens, A. Margaritis, Determination of the volumetric mass transfer coefficient (k, a) using the dynamic "gas out-gas in" method: analysis of errors caused by dissolved oxygen probes, Biotech. Bioeng. 46 (1995) 338–392.